THE CERAMIC CERAMIC

Contents lists available at ScienceDirect

Journal of Materiomics

journal homepage: www.journals.elsevier.com/journal-of-materiomics/



Research paper

Frictional heat-assisted performance enhancement in dynamic Schottky contact of Al/Ag₂Se-based tribovoltaic nanogenerator



Supakarn Worathat ^a, Utchawadee Pharino ^a, Phakkhananan Pakawanit ^b, Arunothai Rattanachata ^b, Rangson Muanghlua ^c, Sugato Hajra ^d, Hoe Joon Kim ^d, Saichon Sriphan ^{a, e, **}, Naratip Vittayakorn ^{a, f, *}

- ^a Advanced Materials Research Unit, School of Science, King Mongkut's Institute of Technology Ladkrabang, Bangkok, 10520, Thailand
- ^b Synchrotron Light Research Institute (Public Organization), Nakhon Rachasima, 30000, Thailand
- c Department of Electronics Engineering, School of Engineering, King Mongkut's Institute of Technology Ladkrabang, Bangkok, 10520, Thailand
- d Department of Robotics and Mechatronics Engineering, Daegu Gyeongbuk Institute of Science and Technology, Daegu, 42988, Republic of Korea
- ^e Faculty of Science, Energy and Environment, King Mongkut's University of Technology North Bangkok, Bangkok, 10800, Thailand
- f Department of Chemistry, School of Science, King Mongkut's Institute of Technology Ladkrabang, Bangkok, 10520, Thailand

ARTICLE INFO

Article history: Received 13 January 2024 Received in revised form 8 February 2024 Accepted 19 February 2024 Available online 24 March 2024

Keywords: Tribovoltaic effect Thermoelectric material Schottky junction Output performance

ABSTRACT

The tribovoltaic nanogenerator (TVNG) has evolved in recent years as a novel type of nanogenerator designed to address the limitations of the standard triboelectric nanogenerator in terms of output signal and charge generation. Besides the outstanding characteristics, the tribovoltaic effect can also well be coupled with another effect to further boost the output performance. In this work, we proposed firstly a frictional heat-assisted performance enhancement in dynamic Schottky contact from the rubbing between n-type silver selenide (Ag₂Se) and aluminum. The chemical composition and physical characteristics of the Ag₂Se ceramic were analyzed using X-ray diffraction, scanning electron microscopy, and Synchrotron X-ray tomography techniques. UV-Vis spectroscopy and UPS were also utilized in order to validate the semiconducting property of the n-type Ag₂Se ceramic. Moreover, the presence of the Schottky junction was demonstrated through the analysis of the current-bias voltage characteristic curve of the Ag₂Se/aluminum (Al) contact under varying stress and temperature conditions. The built-in electric field plays a crucial part in the tribovoltaic effect by efficiently transferring the excited carriers to an external load through sliding contact between Ag₂Se and Al. Demonstrating the synergy between tribovoltaic and thermoelectric effects becomes achievable through the excellent thermoelectric property of Ag₂Se. Herein, the proposed TVNG generated a peak output voltage and current of around 0.7 V and 24.8 nA, respectively, achieving a maximum output power of 12.6 nW at a load resistance of 10 k Ω . The influence of frictional heat on the output performance of the proposed TVNG was well demonstrated by the thermal-induced voltage and enhanced electrical output from continuous sliding. The concepts given in this study establish the basis for the progress of effective energy collection employing semiconducting materials and the advancement of flexible harvesting and sensing device development in the

© 2024 The Author(s). Published by Elsevier B.V. on behalf of The Chinese Ceramic Society. This is an open access article under the CC BY-NC-ND license (http://creativecommons.org/licenses/by-nc-nd/4.0/).

1. Introduction

The rapid progression of human civilization and the need for increased energy consumption have resulted in an urgent energy crisis and environmental issues [1]. Thus, the utilization of sustainable energy from ambient sources for replacing fossil fuels, which are harmful and nonrenewable and lead to global warming, is a significant concern [2]. A triboelectric nanogenerator (TENG) was initially discovered in 2012 by Wang *et al.* [3]. It became a new

Peer review under responsibility of The Chinese Ceramic Society.

^{*} Corresponding author. Advanced Materials Research Unit, School of Science, King Mongkut's Institute of Technology Ladkrabang, Bangkok, 10520, Thailand. ** Corresponding author. Faculty of Science, Energy and Environment, King Mongkut's University of Technology North Bangkok, Bangkok, 10800, Thailand. *E-mail addresses*: saichon.s@sciee.kmutnb.ac.th (S. Sriphan), naratip.vi@kmitl. ac.th (N. Vittayakorn).

energy technology that is lightweight and compact, offers a wide range of material options, and exhibits high energy conversion efficiency. In principle, TENG produces an alternating current (AC) signal *via* contact electrification and electrostatic induction to convert mechanical energy into electricity [4–10]. Recently, the friction of semiconductors with metal (or semiconductors) has brought a new type of mechanical energy harvester called the tribovoltaic effect [11,12]. The energy generated by the friction between atoms during the formation of chemical bonds causes the activation of nonequilibrium carriers. These carriers are then split in a specific direction to create the electric current due to the electric field formed at the junction [12]. The tribovoltaic nanogenerator (TVNG) overcomes the barrier of the TENG by providing the direct current (DC) signal with a high charge density [13].

Recently, many semiconductor material systems have been explored in order to enhance the electric output performance of the TVNGs [14-17]. Thermoelectric materials are a class of materials that can convert heat directly into electricity, and have been rarely used in nanogenerators. The thermoelectric materials that have been extensively studied so far for energy harvesting include metal chalcogenides composed of Bi-Te/Cu-Se/Sn-Se, half-Heusler compounds, multicomponent oxides, PbTe/GeTe hybrids, and organic-inorganic composites [18-21]. For the TVNG, Bi₂Te₃ was first proposed as the tribovoltaic material, acting as one of the semiconductors for contact electrification [22]. The popular of Bi₂Te₃ is due to remarkably anisotropic thermoelectric properties with a narrow bandgap of around 0.1 eV, which has been utilized as an essential component in commercial thermoelectric devices [23,24]. However, the study of the influence of the thermoelectric property Bi₂Te₃ on the tribovoltaic performance is absent. Considering the fact that the element Te is limited in availability and highly expensive, it is of the utmost importance to seek alternatives that are free of Te [25]. An interesting choice is Ag₂Se, an n-type semiconductor that is both inexpensive and friendly to the environment. Ag₂Se also demonstrates excellent thermoelectric performance, in addition to possessing a low thermal conductivity and high carrier mobility at near-room temperatures [26,27].

This research investigated the synergetic effect between tribovoltaic and thermoelectric by continuously sliding Ag₂Se ceramic onto Al. The multi-physics coupling behavior for these effects was investigated systematically in 2021 by Z. Zhang et al. [28], revealing the feasibility for multi-energy collection and sensing. The rubbing between n-type silicon (Si) and metal provides the Schottky interface. Increased sliding velocity and pressure can amplify both the thermo- and tribo-outputs, which are generated by elevated temperature difference and greater frictional energy, respectively. Importantly, expanding the investigation of tribovoltaic and thermoelectric coupling to other semiconductors, especially for thermoelectric semiconductors is highly essential. Herein, the Schottky interface between n-type Ag₂Se and Al serves the DC output. Possibly, it comprises two distinct components: the thermoelectric effect, which accounts for the stable part, and the tribovoltaic effect, which accounts for the fluctuating part. Under the influence of the built-in electric field from the metal-semiconductor interface, as confirmed by Synchrotron radiation UPS and non-linear currentbias voltage characteristic curves, the electron-hole pairs excited by friction are separated to generate a current. During that period, the heat generated by friction causes the majority carrier to move in the direction corresponding to the rising temperature gradient. An equivalent circuit is proposed for expressing the charge generation mechanisms of the coupling effect. Increased sliding velocity produces the thermal-induced voltage and shows the potential to increase the output performance of the TVNG. The purpose of this work is not only to establish a fundamental of multi-physics combination but also to exhibit the possibility of multi-energy

collection and sensing in practical usages. Since the junction interface is a key point for improving the TVNG performance, hence, seeking other thermoelectric materials exhibiting high semiconducting properties with durability at high friction is also highly suggested for future nanogenerator development.

2. Experimental section

2.1. Synthesis of Ag₂Se powders

All reagents were analytical grade and used without further treatments. Chemical precipitation synthesizes the Ag₂Se powders [29]. Firstly, the 0.9478 g of Se (QReCTM) and 1.5125 g of Na₂SO₃ (QReCTM) were dissolved in 120 mL of Deionized (DI) water. The mixed solution was stirred continuously by a magnetic stirrer at 100 °C for 30 min to obtain Sodium selenosulfate (Na₂SeSO₃) according to the chemical reaction:

$$Na_2SO_3 + Se \rightarrow Na_2SeSO_3$$
 (1)

After the Na₂SeSO₃ solution cooled to room temperature (RT), 4.0772 g of AgNO₃ (QReCTM) in 240 mL of DI water was poured into the first solution. After the reaction for 2 h, the precipitate of Ag₂Se was collected and rinsed with DI water and absolute ethanol several times. The reaction followed this chemical reaction:

$$Na_2SeSO_3 + 2AgNO_3 + H_2O \rightarrow Ag_2Se(s) + 2NaNO_3 + H_2SO_4$$
 (2)

The final samples were dried in a vacuum oven at 70 $^{\circ}$ C for 24 h. The Ag₂Se powders were then obtained.

2.2. Preparation of Ag₂Se ceramic

Fig. 1a illustrates the fabrication of Ag_2Se ceramics. Ag_2Se powder 1.98 g mixed with 3 drops of PVA binder (PVA binder conc. 5% (mass by volume percentage (w/v): mass by volume percentage refers to the mass of solute (in grams) present in 100 mL of solution.) in DI water) in a pestle and agate mortar for 3 min. Then the Ag_2Se mixture was shaped to pellet (diameter = 1 cm, thickness = 0.4 cm) in a tungsten carbide block, and subjected to uniaxial pressure of 7,000 kPa at RT for 10 min for densification. Finally, Ag_2Se ceramics were removed from the block, and sintered at 250 °C at a rate of 5 °C/min for 10 min in a nitrogen atmosphere.

2.3. Fabrication of the TVNG based on Al/Ag₂Se interface

The structure of the TVNG based on Al/Ag₂Se interface is shown in Fig. 1b. The device structure consists of n-type Ag₂Se ceramic pairing with aluminum. The electrodes are conducted with silver electrodes and copper wires. The automatic linear motor applies the sliding motion to the metal horizontally with the fixed position of ceramic to produce the electrical signals.

2.4. Characterizations

The purity and crystal structure of prepared samples were examined by X-ray diffraction (XRD) recorded by D8 Advance X-ray diffraction (Bruker company, Germany) with a diffractometer employing Cu $\rm K_{\alpha}$ radiation in the 2θ range from 20° to 60° . The surface morphology with energy dispersive X-ray spectroscopy (EDS) and optical absorbance of the samples were characterized using scanning electron microscopes (SEM) (FEI, Helios Nano Lab G3 CX), and UV–Vis Spectrophotometers (HITACHI, UH4150) ranging from 200 nm to 800 nm, respectively. The binding energy scale was calibrated from adventitious carbon using the C1s peak at

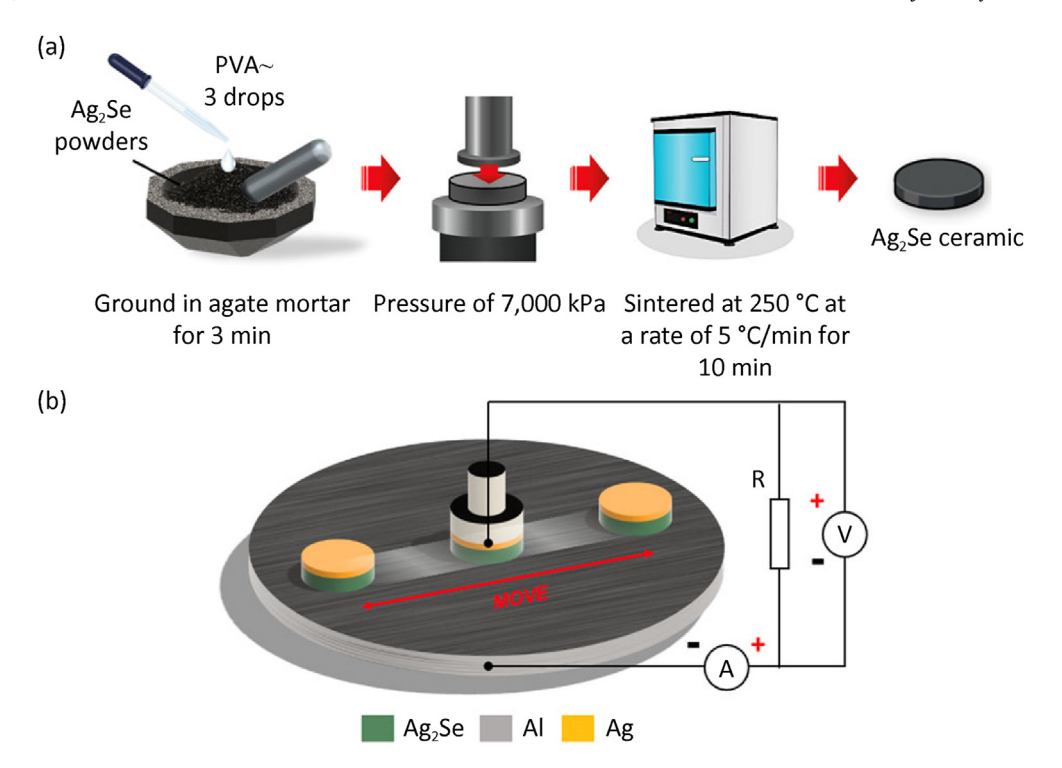


Fig. 1. (a) Preparation of n-type Ag₂Se ceramic; (b) A 3D schematic showing the experimental setup and structure of the TVNG based on the Al/Ag₂Se interface.

284.8 eV.

Synchrotron radiation X-ray tomographic microscopy (SRXTM) was carried out at beamline BL1.2 W at SLRI, Thailand. The X-ray Synchrotron radiation was produced by a 2.2-T multipole wiggler running at 150 mA and 1.2 GV in the Siam Photon Source. With a source-to-sample distance of 34 m and a mean energy of 12.5 kV, filtered polychromatic X-ray beams were used for all SRXTM studies. The detection equipment, comprising a lens-coupled X-ray microscope (Optique Peter, France), a 200-µm-thick YAG: Ce scintillator (Crytur, Czech Republic), and a sCMOs camera (pco.edge 5.5, $2,560 \times 2,160$ pixels, 16 bits), provided the X-ray projections of the materials. At an isotropic voxel size of 1.44 µm, the tomographic images were obtained. Following data acquisition, a flat-field correction procedure was used to normalize the X-ray projections, and Octopus reconstruction software was utilized to reconstruct them [30]. Drishti software was used to compute segmentation analysis and a three-dimensional representation of the samples' tomographic volumes [31]. Synchrotron radiation photoemission spectroscopy (SRPES) was accomplished at beamline BL3.2Ua: PES at SLRI, Thailand. The beamline produces photons with energies ranging from 39 to 160 eV, 220-520 eV, and 440-1,040 eV utilizing 600 lines/mm grating, 1200 lines/mm grating and 2400 lines/mm grating, respectively. Approximately 1.0×10^{10} photon/s was the photon flux at the sample. The size of the photon beam was 200 $\mu m \times 200~\mu m$. An angle-integral hemispherical electron analyzer (Alpha 110, Thermo VG Scientific), positioned at a 90° angle from the incident photon beam (39.5 eV), was installed in the chamber. In the analysis chamber, the pressure was $\sim 10^{-10}$ mbar. Various kinetic energies of photons ranging from 32 to 46 eV and 5–15 eV were used to trace the secondary electron cut-off and valence band (VB) spectra, respectively. The recording conditions were at pass energy (PE) of 10 eV, dwell time of 100 ms, and step size of 0.02. A small bias of -9.6 V is applied to the samples to deconvolute the true work function by shifting the entire UPS signal to the higher kinetic energy.

The experiment was designed to record the output voltage and current from the TVNG based on the Al/Ag₂Se interface at RT. The metal was attached to the slider operated by a linear motor with a sliding speed of ~16 mm/s and a sliding distance of ~15 mm, while the Ag₂Se ceramic was attached to the substrate in static position. The current-bias voltage characteristic curves of the Al/Ag₂Se interface were measured at RT between -1 V and +1 V at various applied vertical forces of approximately 0–5 N with the contact area of the test of about 5 cm², and at different temperatures (30–100 °C) via a precision LCR meter (E4980A, Agilent). A pair of thermocouples (K-type) connected to a temperature recorder (449SD, Ponpe) were used to monitor the temperature variation between the hot and cold sides. Thermographic inspection during sliding of the TVNG was achieved by using a thermal imaging camera (HT32, HT Instruments). The output voltage and current of the TVNG were recorded via a digital oscilloscope (DSOX1202A, Keysight) and a picoammeter (6485/E, Keithley), connected to a computer with real-time data acquisition software and controlled a relative humidity (RH) of 50%.

3. Results and discussion

The phase purity and crystallinity of Ag₂Se ceramic were observed using XRD, as shown in Fig. 2a. The XRD pattern indicates the orthorhombic phase (β -Ag₂Se) for all samples with two prominent diffraction peaks at 2 θ of 33.5° and 34.7°, corresponding to the (112) and (121) reflective planes, respectively. The pattern is in good agreement with the literature data for β -Ag₂Se (the standard JCPDS card file, 24–1041). Since the orthorhombic phase is a low-temperature stable phase, it is logical to produce the orthorhombic phase at low temperatures (~250 °C) [29,32,33]. However, the slight broadening peaks shown in the XRD pattern may reflect the smaller crystalline size (~(8.00 \pm 0.16) nm) of the products. It should be noted that there are some small impurity peaks (30° and 50°) that occurred from the PVA binder not fully evaporating by

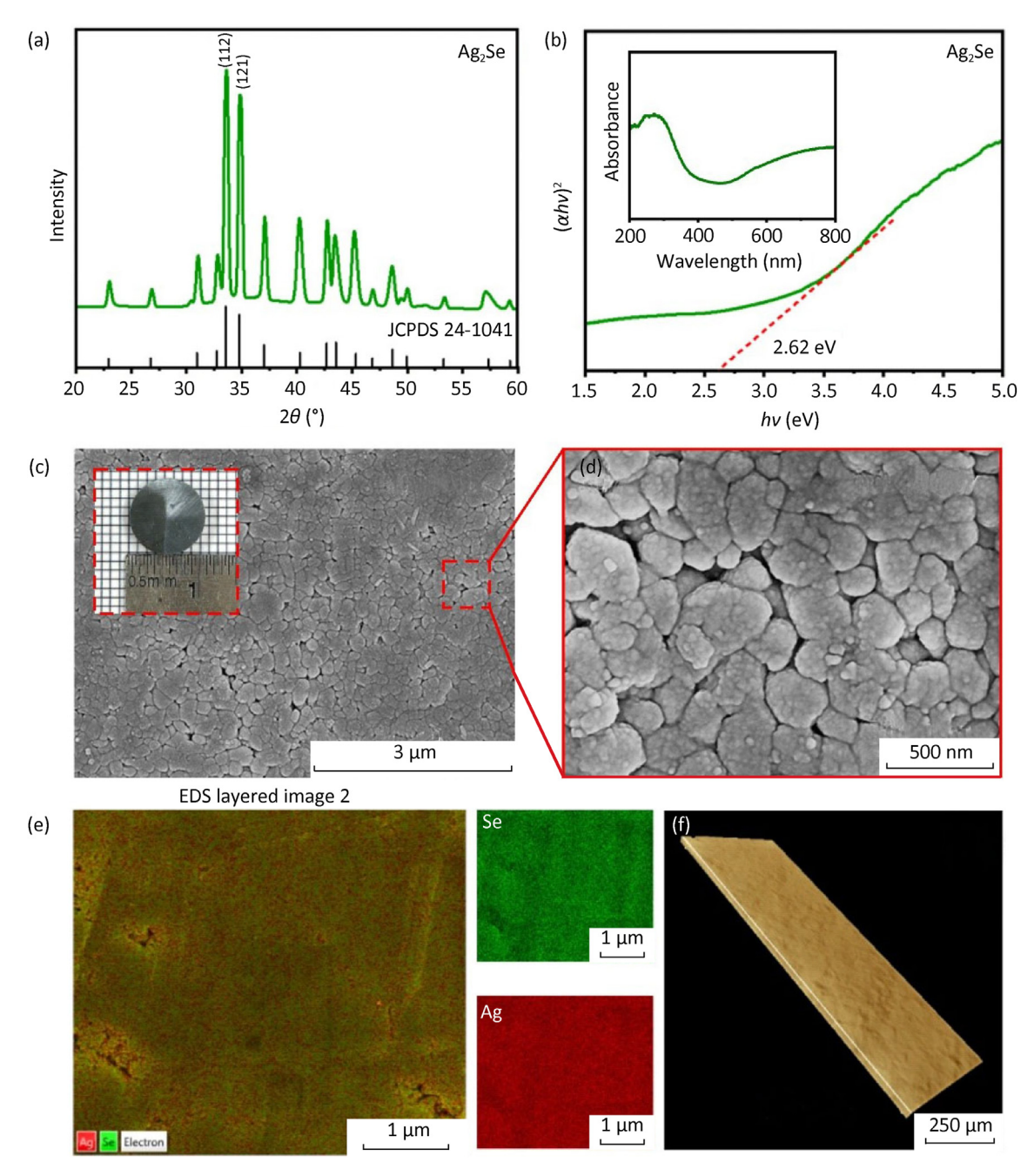


Fig. 2. (a) XRD pattern; (b) UV-Vis absorbance spectra and Tauc plot; (c, d) SEM micrographs; (e) EDS mapping for total elements; (f) 3D visualization of the Ag₂Se ceramic.

ceramic sintering. However, this does not affect the tribovoltaic performance since it mainly relies on the contact interface and semiconducting properties of the material [12,13].

The UV–Vis absorption spectra in the region of 200–800 nm (Fig. 2b) was used to examine the optical characteristics of Ag_2Se . Absorption is highly strong around the ultraviolet and visible regions of the spectra [34]. The optical band gap E_g of the Ag_2Se can be determined by Tauc's plot [35]:

$$\alpha h v = K (h v - E_g)^n \tag{3}$$

where α is the absorption coefficient, hv is the photon energy, K is the constant, and n is the constant (n equals to 1/2 or 2 for direct

and indirect semiconductor, respectively). By extrapolating the straight line of the relationship between $(\alpha h v)^2$ and h v, the optical band gap of Ag₂Se was found to be 2.62 eV. This value is well corresponding to the value reported by Ref. [36].

Fig. 2c and d show the SEM images to reveal the surface structure of the Ag₂Se ceramic at magnifications of $30,000\times$ and $100,000\times$, respectively. The morphology of prepared ceramic was slightly porous, and had a small grain size of approximately (0.876 ± 0.410) µm. The results found a nonuniform size distribution in the presence of microstructural inhomogeneity due to the polycrystalline structure of the ceramic [37]. The relative density $\rho_{\rm r}$ of the Ag₂Se ceramic can be calculated using eq. (4) [38]:

$$\rho_{\rm r} = \frac{4m}{\pi d^2 h \rho_{\rm r}} \tag{4}$$

where m is the mass of Ag₂Se, d and h are the diameter and thickness of the ceramic, respectively, and ρ_t is the theoretical density of Ag₂Se (8.22 g/cm³). The Ag₂Se ceramic sintered at 250 °C for 10 min has a diameter of 0.91 cm, thickness of 0.36 cm, and a mass of 1.96 g. The calculated ρ_r reached 92.1%, confirming the densification of the prepared ceramic. Furthermore, we performed EDS measurements to qualitatively assess the Ag₂Se ceramic composition and the elemental distributions of Ag and Se. The results are shown in Fig. 2e. The silver and selenium atoms were distributed uniformly, and no element precipitates were observed [39]. The densification and phase uniformity are also confirmed by SRXTM technique (Fig. 2f). SRXTM is a non-invasive method used to examine and display the internal characteristics of solid objects that cannot be seen through. It enables the creation of a threedimensional image of internal structures by detecting variations in the way energy waves interact with the structures [40]. In this case, the utilization of this technique enabled us to comprehensively survey the entire expanse of the landscape within an approximate area of 0.25 mm \times 1.00 mm of the specimen. The 3D images illustrated a well-distributed phase of the silver and selenium mixture, and revealed a high densification of the prepared ceramic.

To verify the Schottky junction effect, the current-bias voltage characteristics of the Al/Ag_2Se static junction in different testing conditions are measured. For load pressures and temperatures applying to the proposed diode (Fig. 3a and b), the rectification behavior was well confirmed for both conditions. The reduction of

Schottky barriers due to forward bias speeds up injection and transportation across the device, resulting in a high current. When the bias is reversed, the voltage-induced rise in barrier height makes it harder for the carriers to inject, resulting in only a somewhat continuous current flow in the device [15]. As illustrated in Fig. 3a, when applying load pressures ranging from approximately 0-5 N vertically to the diode, the current level rises noticeably as compared to the immaculate level (0 N). The increasing trend refers to the improved electrical outputs, i.e., voltage and current, of the nanogenerators [41,42], since the TVNG performance is based on the interfacial electric field [13]. Larger currents are usually the result of higher levels of stress applied to the junction due to the alteration of the band structure [43]. Additionally, the non-linear characteristic curves of the Al/Ag₂Se diode in the temperature range of 30–100 °C are recorded (Fig. 3b). The curve shifts downward on the lower bias side with an increase in temperature. More electrons have the energy to overcome the greater barriers as the temperature rises [44,45]. The occurrence trend therefore indicates the strong temperature-dependency of the metal-semiconductor contact.

UPS measurements were performed to determine the work function (WF) and the ionized energy of the valence band energy (E_V) with respect to the Fermi level (E_F) [46]. The technique is crucial for determining the charge generation and transfer behaviors of the TVNG and other energy harvesters [17,47]. The UPS spectra of Al and Ag₂Se ceramic in the high binding energy (BE) region are depicted in Fig. 3c. Theoretically, the WF equals the difference between the incident photon energy (hf = 39.5 eV) and the binding energy of the secondary electron cut-off [48,49]. Therefore, the spectra give the WF information of 4.10 eV and 5.23 eV for Al and Ag₂Se ceramic, respectively, which are well

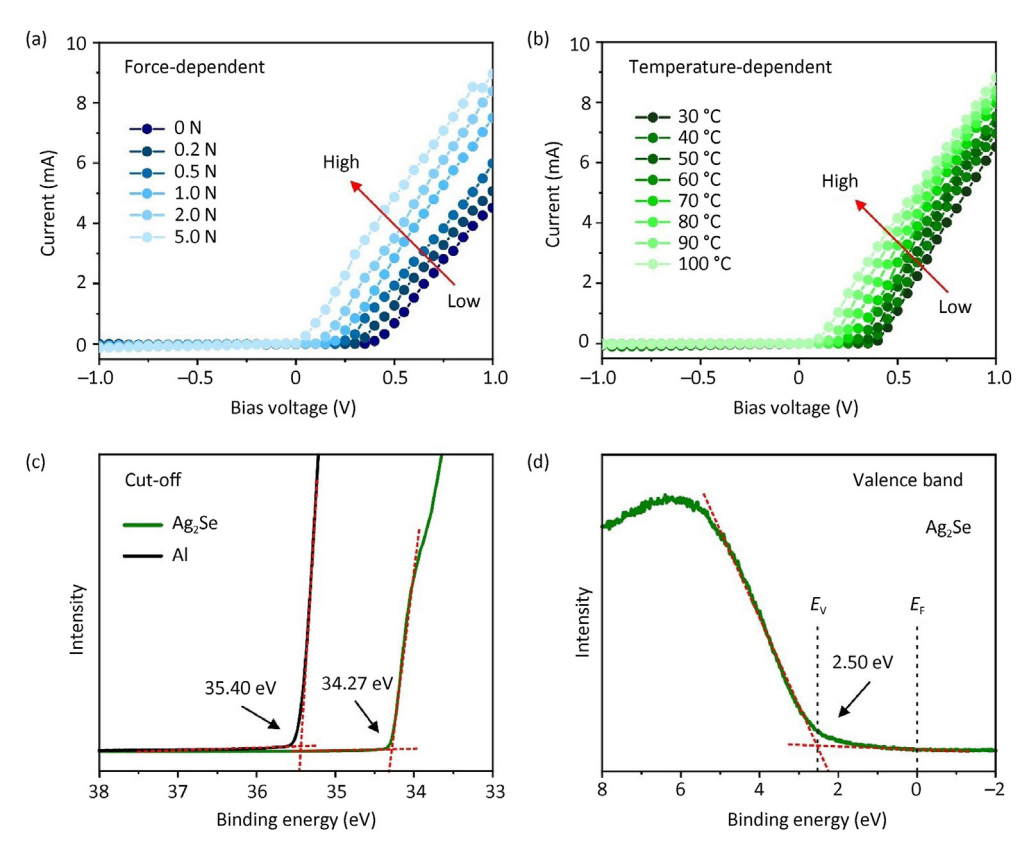


Fig. 3. Current—bias voltage characteristic curves of Al/Ag₂Se Schottky junction at different (a) applied forces, and (b) operation temperatures; UPS spectra at (c) secondary electron cut-off for Al and Ag₂Se, and (d) valence band maxima relative to the Fermi-level for Ag₂Se.

related to the previous works [50,51]. Additionally, at the low binding energy region, the UPS reveals the valence band maximum associated with the ionized energy with respect to the Fermi level (BE = 0 eV) [48]. As shown in Fig. 3d, the Ag₂Se ceramic shows the difference between E_V and E_F of 2.50 eV. The large $|E_V - E_F|$ with respect to its band gap proves explicitly the n-type property of the Ag₂Se [52].

The electronic parameters obtained from UV-Vis and UPS characterizations are used to draw the band energy diagrams of the contact Al/Ag₂Se corresponding to the mechanism based on the tribovoltaic effect. Three working processes of the TVNG based on the Al/Ag₂Se interface are shown in Fig. 4a. The interface between Ag₂Se and Al is separated in a non-contact state (Fig. 4a-i) with the vacuum level (E_0) , conduction band (E_C) , valence band (E_V) , and Fermi levels of Ag₂Se (E_{FS}) and Al (E_{Fm}). In this case, the WF of Ag₂Se is larger than that of Al, leading to downward band bending with a barrier height of ~1.13 eV when they are in contact (Fig. 4a-ii). The formation of Schottky junction is found from the alignment of two Fermi levels. In a static condition, there is no generation of an output signal due to the absence of excitation energy. However, when Ag₂Se and Al rub against each other, electron-hole pairs can be produced in the space charge region. According to the tribovoltaic effect [12,15], the dissipation energy from friction (E_{friction}) can be absorbed by electrons. There is the driving up of excited electrons to E_C , followed by the drift of holes along the built-in electric field ($E_{\rm field}$) to generate a DC current signal $I_{\rm DC}$ (Fig. 4a–iii). The continuous sliding can produce heat (E_{heat}) at the metal-semiconductor interface, resulting in a temperature gradient throughout the system [28]. This assists the common sliding energy for further improvement of the total charge density of the TVNG due to the more released bindingtons [12,13].

Based on the above mechanism, the equivalent circuit diagram of the TVNG is drawn in Fig. 4b. As inspired by a solar cell model [53,54], the nanogenerator can be simplified into four elements: a current source, a diode, and two resistors. In this case, the current source Is expresses the production of charge carriers in the semiconductor layer of the tribovoltaic cell due to incoming energy. The currents I_F and I_H are the current sources occurred by frictional and thermal energies, respectively. The shunt diode demonstrates the unidirectional charge transfer from the built-in electric field. The shunt resistor R_P indicates the presence of high-current pathways within the semiconductor caused by mechanical imperfections and material dislocations. The series resistor R_S represents the presence of resistance at the outside areas of the semiconductor, particularly at the point where the semiconductor and metal electrodes connect. In the non-contact state, two tribovoltaic materials are being separated, representing the turn-off of the switch. When two materials are in contact and sliding, the switch state is turned-on. There is the production of electric current I_{DC} and voltage V_{DC} to external load R_L. Applying the Kirchhoff's current law and Shockley diode equation to the circuit, yields the characteristic equations [53]:

$$I_{DC} = I_S - I_D - I_P \tag{5}$$

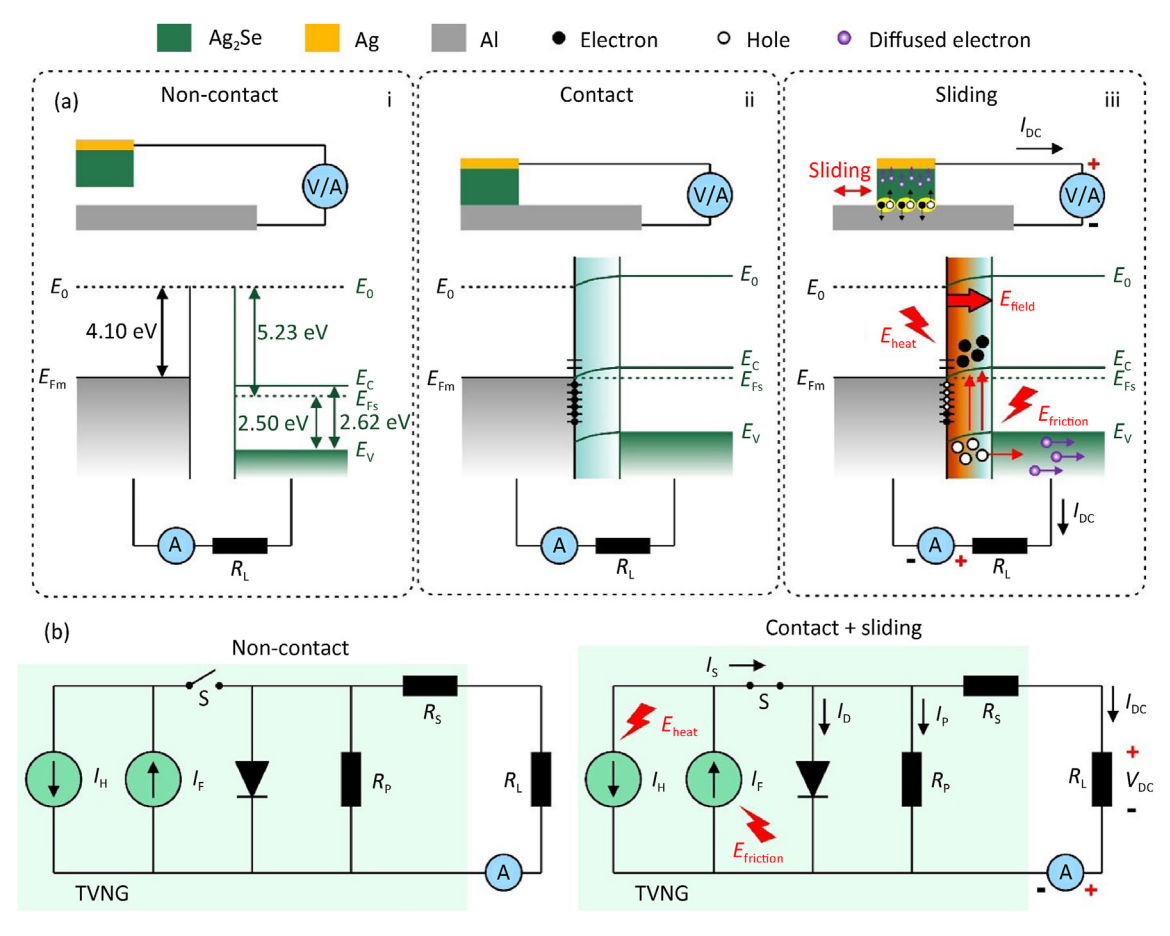


Fig. 4. Working process with electronic band diagrams of the TVNG based on Al/Ag₂Se interface in (a) non-contact, contact, and sliding states; (b) Proposed equivalent circuit for the TVNG during operation.

$$I_{DC} = I_{S} - I_{o} \left[\exp \left\{ \frac{V_{DC} + I_{DC}R_{S}}{nV_{T}} \right\} - 1 \right] - \frac{V_{DC} + I_{DC}R_{S}}{R_{P}}$$
 (6)

$$I_{S} = I_{F} - I_{H} \tag{7}$$

where n is the diode ideality factor, and V_T is the thermal voltage. The equations state that reduction of R_S and increase of R_P are the factors to gain higher performance [54]. For the TVNG, input energy sources can be thermal and frictional energies affecting the generation of I_S . The direction of I_F is in the opposite direction of I_H due to the different nature of charge generation mechanisms. The thermoelectric effect diffuses the excess charges to the electrode from the hot side to the cold side, obeying the temperature gradient [55]. However, the direction of tribovoltaic charge transfer follows the direction of the built-in electric field at the interface [13]. In this case, the formation of built-in electric field is from metal to semiconductor (Fig. 4a), the electric current generated from frictional energy flow in a different direction of thermal energy. Therefore, eq. (7) can be manipulated, and indicates the amount and direction of charge transfer to the external load. The experimental verification will be demonstrated later.

As shown in Fig. 5a, during continuous sliding, the frictional heat occurs at the metal-semiconductor interface. The heat convection provides the temperature gradient ($\Delta T = T_{\rm H} - T_{\rm C}$) between the hot and cold sides, promoting the coupling between the tribovoltaic and thermoelectric effects of the TVNG [28,56]. The convection is generally transferred from high to low temperatures, where the metal shows a higher thermal conductivity than the semiconductor [57]. In this work, therefore, we attached the thermoelectric probes at the electrode of Ag₂Se ceramic (probe 1) and at the position of Al near the interface (probe 2) to define the cold and hot sides, respectively. The energy dissipation at the interface produces the relative heat flux $Q_{\rm R}$ in tiny segment through mechanical friction according to eq. (8) [58]:

$$Q_{R} = \begin{cases} Q & (x,y) \in S \\ h(T_{A} - T) & \text{else} \end{cases}$$
 (8)

$$Q = \mu P \cdot v \tag{9}$$

where O is the heat flux occurred in a specific area, h is convective heat transfer coefficient, $T_A - T$ is the temperature difference between ambient temperature and field temperature that occurred at the specific contact area during the sliding of the TVNG, (x, y) is the coordinate vector, S is the contact surface, μ is the friction coefficient, P is the pressure, and v is the sliding velocity. This demonstrates that increasing the velocity of sliding causes an increase in temperature at the metal-semiconductor interface. A temperature gradient leads to the diffusion of excited carriers to the electrode. At the same time, this couples the excited charges from friction, which is essential for boosting the final output energy [28]. To verify the heat generated at the interface during sliding, we use 2D finite element analysis by Ansys software to simulate the phenomenon that occurs at the interface during contact sliding. For the model, structural-related materials, i.e., Ag₂Se and Al, with the same size as the experiment were constructed based on the tribovoltaic effect. The setting speed is 16 mm/s, load force is 0.2 N, convection heat coefficient is 1 W/(m²•°C), and environmental temperature is 26 °C. The simulated distribution of temperature during sliding for 1 cycle of the TVNG based on the Al/Ag₂Se interface is shown in Fig. 5b. Increasing the sliding distance serves the heat fluctuation at the interface, and rapidly transfers to the end of materials following their thermal conduction property. Further increasing the sliding cycle, the simulated ΔT greatly increases, which is in good agreement with experiment result (Fig. 5c). The additional confirmation of heat diffusion during sliding of the TVNG is shown in Fig. 5d. Thermographic image well illustrated the temperature difference $(\Delta T \sim 0.7 \, ^{\circ}\text{C})$ between the top of Ag₂Se and Al as the positions of probe 1 and 2, respectively.

With a contact area of ~0.79 cm² (diameter of Ag₂Se

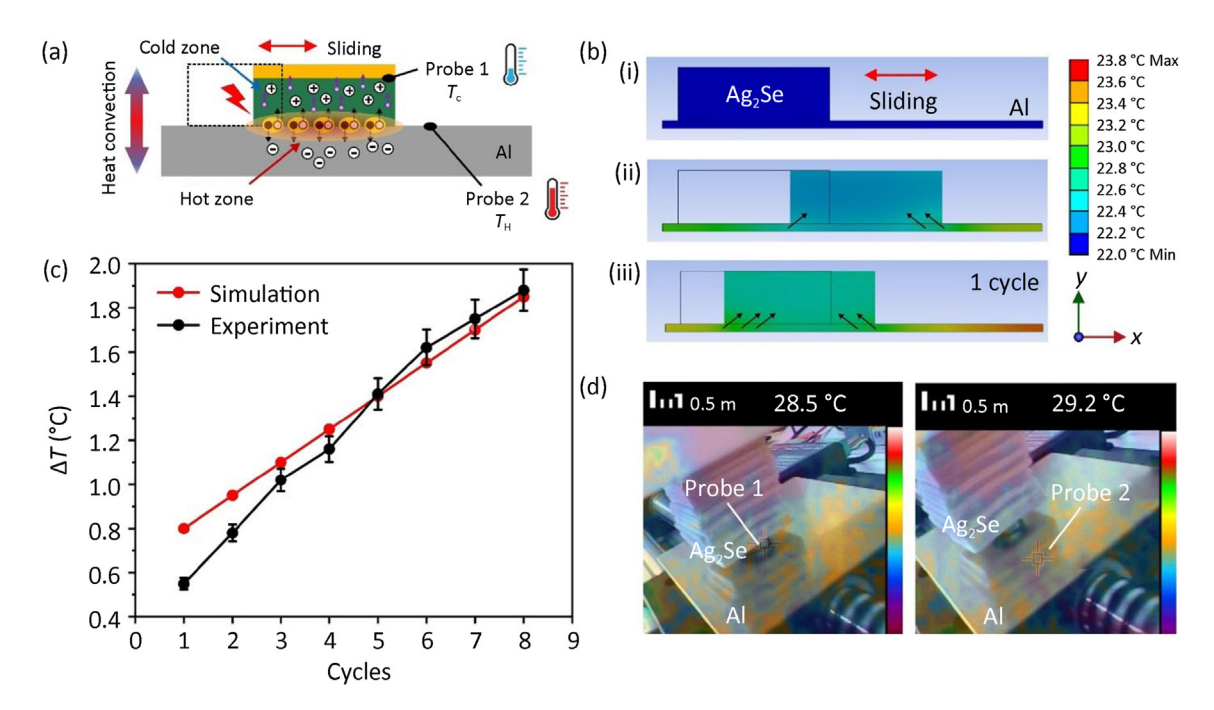


Fig. 5. (a) Working mechanism showing the coupling of tribovoltaic and thermoelectric effects by frictional heat during sliding; (b) The simulated heat convection for the sliding contact between Ag₂Se and Al for 1 cycle; (c) The temperature difference between two probes compared by experiment and simulation; (d) Thermographic pattern during sliding of TVNG.

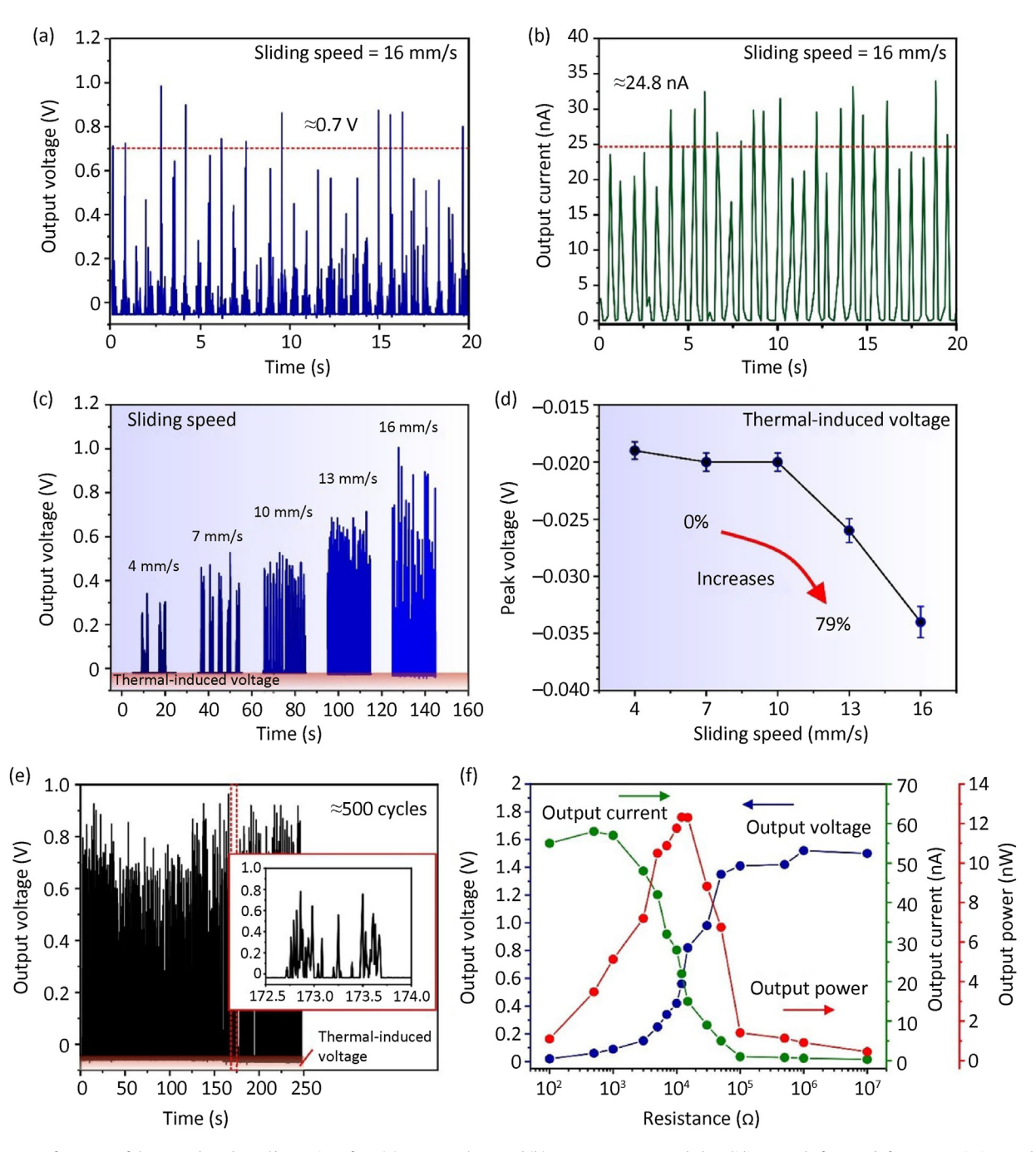


Fig. 6. Output performance of the TVNG based on Al/Ag_2Se interface. (a) Output voltage and (b) output current recorded at sliding speed of 16 mm/s for 20 s; Variation tendencies of (c) output voltage and (d) peak voltage of the TVNG at different sliding speeds; (e) Output voltage signal of the TVNG recorded for 250 s; (f) Output voltage, output current and calculated output power of the TVNG at various external load resistances.

ceramic = 1 cm²), as shown in Fig. 6a and b, the TVNG based on the Al/Ag₂Se interface could generate the average DC output voltage and current of approximately 0.7 nA and 24.8 nA, respectively, with controlled sliding speed of 16 mm/s, maximum sliding distance of 15 mm and contact force of 0.2 N. In the current work, to study the tribovoltaic and thermoelectric performances of the TVNG, we are focusing on the basic sliding process with a constant force and no external heat. When the sliding velocity increases from 4 to 16 mm/s, the average output voltage increases from 0.3 V to 0.7 V (Fig. 6c). Higher motion velocity leads to higher output performance, according to other literatures [59–61]. More dissipated frictional energy from faster sliding results in more electrons and holes being

excited at the metal-semiconductor interface [60,61]. The low output current is due to the thick ceramic (~0.33 cm), which provides the high charge recombination [62]. The unstable outputs could be treated by the nature of electroceramic, which has a polycrystalline structure differing from the semiconducting single crystal [63]. During sliding, hence, there is a possibility to tailor the surface structure at the interface, affecting the generated electrical signal. Another point relates to the mismatch of the contact surface between Al and Ag_Se. Hence, the careful alignment of the material's surface as well as the setup are important. More investigation to improve the stability will be considered in the future work.

Table 1 shows the comparison of the proposed TVNG with the

Table 1 Comparison of output performance among various Schottky junction-based TVNGs [16,28,41,60,64—68].

Pair of contact materials	Force/speed	Approximated $oldsymbol{V_{avg,p}}/I_{avg,p}$	Instantaneous Power density	Key effect	Ref.
Mo tip	50 MPa	Not available	Not available	Schottky	[64]
/annealed TiO ₂	/10 μm·s ⁻¹	/1.3 nA			
Cu/n-Si	9 N	2.23 mV	Not available	Schottky/thermoelectric	[28]
	/12 cm·s ⁻¹	/2.16 μA			
W tip/WO ₃	0.3 N	Not available	Not available	Schottky	[16]
	/2.7 cm·s ⁻¹	/2.5 nA			
Au tip/n-Si	250 μΝ	138.5 mV	7 W⋅m ⁻² Schottky	Schottky	[66]
	/4.3 μm·s ⁻¹	/3.5 nA	@80 MΩ		
Steel ball/n-Si	1 N	470 mV	3.7 mW⋅m ⁻²	Schottky	[65]
	/1 Hz	/32.3 nA	@7 MΩ		
Stainless steel	15 N	0.33 V	Not available	Schottky	[41]
/n-Si	/38.7 cm·s ^{−1}	/16 μΑ			
Al	0.01 MPa	0.56 V	1.7 μW∙cm ⁻²	Schottky	[60]
/PEDOT:PSS	/3 cm⋅s ⁻¹	/81.28 nA	@10 kΩ		
Al alloy	5 N	0.84 V	11.67 mW⋅m ⁻²	Schottky	[67]
/PEDOT:PSS	/30 cm·s ⁻¹	/309 µA	@20 kΩ		
Al	3 N	3.69 V	Not available	Schottky	[68]
/CsPbBr ₃	/70 cm⋅s ⁻¹	/5.5 μA		/photovoltaic	
Al	0.2 N	0.7 V	15.95 nW \cdot cm ⁻²	Schottky	This work
/Ag ₂ Se	/16 mm·s ⁻¹	/24.8 nA	@10 kΩ		

^{*}Mo = molybdenum, Cu = copper, Si = silicon, W = tungsten, Au = gold

recent TVNGs based on the Schottky interface [16,28,41,60,64–68]. For the most related works, our device shows comparable performance with the dielectric TiO2 [64], and the coupled tribothermoelectric effect-based TVNG [28]. Also, the present TVNG based on the Al/Ag₂Se interface reaches a higher performance than various nanogenerators using n-Si and metal tips (or steel ball) for tribovoltaic sliding [16,65,66]. Even though the output current is lower, our TVNG shows a higher output voltage than the TVNG based on the stainless steel/n-Si interface [41]. Additionally, in the case of organic semiconductor and halide perovskite as novel materials for the TVNG [60,67], the proposed device also demonstrates comparable output performance with the PEDOT:PSS-based TVNGs [60,67], even though the contact force and sliding speed are much lower. However, the recorded outputs are still lower than the dynamic Al/CsPbBr₃ TVNG [68], which employs higher carrier production from a higher frictional load and operation speed.

Herein, the possible coupling effect can be achieved in two steps. Firstly, at the initial rubbing, the tribovoltaic effect plays the main role in producing the charges. Secondly, continuous sliding causes the heat at the interface. The heat convection generates additional charges following the thermoelectric effect until it reaches a stable temperature gradient. Apart from a common tribovoltaic effect, due to the good thermoelectric property of Ag₂Se [52], the Seebeck effect well causes the temperature differential to create a thermal electromotive force between two contact materials as [28]:

$$V = \frac{1}{e} \int_{T_{c}}^{T_{H}} (SdT)_{\text{semi}} - \frac{1}{e} \int_{T_{c}}^{T_{H}} (SdT)_{\text{metal}}$$
 (10)

where *S* is the Seebeck coefficient. Nevertheless, the Seebeck coefficient of metal is much smaller than that of semiconductors. Hence, the latter term of eq. (10) can be ignored, and the main influence of charge generation obeys mainly the semiconductor. Interestingly, at high speed of rubbing, there is a generation of thermal-induced voltage with respect to the temperature accumulated at the interface from sliding. This voltage exhibited the opposite direction from the signal generated by the tribovoltaic effect, confirming initially the synergetic effect between the tribovoltaic and thermoelectric effects. The static potential in the negative region can be interpreted from the role of the built-in

electric field located at the metal-semiconductor junction (Fig. 4). Elevated temperature directly affects the electronic parameters, e.g., band gap, and carrier mobility [69,70], thereby configuring the junction potential. As shown in Fig. 6d, the increasing rate of thermal-induced voltage reached about 79%. Additional evidence could be found by further sliding for 250 s (~500 cycles) (Fig. 6e), proving the influence of frictional heat on the output performance of the proposed TVNG. To illustrate the potential for utilizing this concept in practical situations, the output voltage and current data as a function of the external resistances of the TVNG based on the Al/Ag₂Se interface have been measured as shown in Fig. 6f. It can be clearly seen the trends of increasing voltage and decreasing current with an increasing resistance [2]. The calculated output power curve showed a peak power of approximately 12.6 nW (~15.95 nW/ cm²) around 10 k Ω , which is highly close to the energy harvester's internal resistance.

4. Conclusions

In conclusion, we showed how frictional heat can improve the performance of a dynamic Schottky contact-based TVNG by rubbing silver selenide (Ag₂Se) and aluminum together. The chemical structure and surface morphology of the Ag₂Se ceramic were carried out using XRD, SEM, and XTM techniques. We clarified the high purity and densification of the prepared semiconducting ceramic. The semiconducting property of the Ag₂Se ceramic was confirmed by UV-Vis spectroscopy and UPS. The Ag₂Se semiconductor provided a band gap of approximately 2.62 eV. Through the UPS technique, an electronic band diagram of Ag₂Se and Al was drawn accurately by the obtained WF and $|E_V-E_F|$. The results prove the ntype property of Ag₂Se, and give essential information for interpreting the charge generation mechanism of the TVNG. Furthermore, the evidence of the Schottky junction was proved by the measurement of the current-bias voltage characteristic curve of the Ag₂Se/Al contact in different force and temperature conditions. Operating via a tribovoltaic effect, the built-in electric field can sweep the excited carriers to external load from sliding. Thanks to an excellent thermoelectric property of Ag₂Se, the coupling between tribovoltaic and thermoelectric effects was demonstrated. The temperature gradient generated during continued sliding provides the additional charges supporting excited charges from the tribovoltaic effect. By paring Ag_2Se and Al, the TVNG produced the maximum output voltage and current of approximately 0.7 V and 24.8 nA, respectively, with a maximum output power of 12.6 nW at a load resistance of 10 k Ω . The thermal-induced voltage exhibited a noticeable rise up to 250 s (about 500 cycles), providing evidence of frictional heat's impact on the proposed TVNG's output performance. The concepts presented in this study lay the foundation for advancing efficient energy harvesting using semiconducting materials. This coupling effect is essential for the future progress of flexible harvesting and sensing devices.

Declaration of competing interests

The authors declare that they have no known competing financial interests or personal relationships that could have appeared to influence the work reported in this paper.

Acknowledgments

The research conducted by S. Sriphan was funded by King Mongkut's University of Technology North Bangkok, Contract no. KMUTNB-67-KNOW-02, and by National Science, Research and Innovation Fund (NSRF), and King Mongkut's University of Technology North Bangkok (Project no. KMUTNBeFFe67-B-35). The work of S. Hajra and H. J. Kim was supported by the Basic Science Research Program through the National Research Foundation of Korea (NRF) (2021R1C1C1011588).

References

- Sriphan S, Vittayakorn N. Hybrid piezoelectric-triboelectric nanogenerators for flexible electronics: recent advances and perspectives. J Sci Adv Mater Dev 2022:7:100461.
- [2] Sriphan S, Charoonsuk T, Maluangnont T, Vittayakorn N. High-performance hybridized composited-based piezoelectric and triboelectric nanogenerators based on BaTiO₃/PDMS composite film modified with Ti_{0.8}O₂ nanosheets and silver nanopowders cofillers. ACS Appl Energy Mater 2019;2:3840-50.
- [3] Fan F-R, Tian Z-Q, Wang ZL. Flexible triboelectric generator. Nano Energy 2012;1:328–34.
- [4] Xu C, Wang AC, Zou H, Zhang B, Zhang C, Zi Y, et al. Raising the working temperature of a triboelectric nanogenerator by quenching down electron thermionic emission in contact-electrification. Adv Mater 2018;30:1803968.
- [5] Lu CX, Han CB, Gu GQ, Chen J, Yang ZW, Jiang T, et al. Temperature effect on performance of triboelectric nanogenerator. Adv Eng Mater 2017;19:1700275.
- [6] Pharino U, Sinsanong Y, Pongampai S, Charoonsuk T, Pakawanit P, Sriphan S, et al. Influence of pore morphologies on the mechanical and tribo-electrical performance of polydimethylsiloxane sponge fabricated *via* commercial seasoning templates. Radiat Phys Chem 2021;189:109720.
- [7] Sriphan S, Pharino U, Charoonsuk T, Pulphol P, Pakawanit P, Khamman O, et al. Tailoring charge affinity, dielectric property, and band gap of bacterial cellulose paper by multifunctional Ti₂NbO₇ nanosheets for improving triboelectric nanogenerator performance. Nano Res 2023;16:3168–79.
- [8] Hajra S, Padhan AM, Panigrahi BK, Pakawanit P, Jagličić Z, Vittayakorn N, et al. Unleashing the potential of morphotropic phase boundary based hybrid triboelectric—piezoelectric nanogenerator. J Materiomics 2023.
- [9] Ou-Yang W, Liu L, Xie M, Zhou S, Hu X, Wu H, et al. Recent advances in triboelectric nanogenerator-based self-powered sensors for monitoring human body signals. Nano Energy 2024;120:109151.
- man body signals. Nano Energy 2024;120:109151.
 [10] Tian Z, Li J, Liu L, Wu H, Hu X, Xie M, et al. Machine learning-assisted self-powered intelligent sensing systems based on triboelectricity. Nano Energy 2023:113:108559.
- [11] Wang ZL, Wang AC. On the origin of contact-electrification. Mater Today 2019;30:34-51.
- [12] Sriphan S, Vittayakorn N. Tribovoltaic effect: fundamental working mechanism and emerging applications. Mater Today Nano 2023;22:100318.
- nism and emerging applications, Mater Today Nano 2023;22:100318.
 [13] Lin S, Wang ZL. The tribovoltaic effect. Mater Today 2023;62:111–28.
- [14] Ren L, Yu A, Wang W, Guo D, Jia M, Guo P, et al. P-n junction based directcurrent triboelectric nanogenerator by conjunction of tribovoltaic effect and photovoltaic effect. Nano Lett 2021;21:10099–106.
- [15] Sriphan S, Worathat S, Pharino U, Chanlek N, Pakawanit P, Choodam K, et al. Highly flexible tribovoltaic nanogenerator based-on p-n junction interface: comparative study on output dependency dominated by photovoltaic effect in freestanding-mode. Adv Funct Mater 2023;33:2305106.
- [16] Šutka A, Zubkins M, Linarts A, Lapčinskis L, Malnieks K, Verners O, et al. Tribovoltaic device based on the W/WO₃ Schottky junction operating through

- hot carrier extraction. J Phys Chem C 2021;125:14212-20.
- [17] Luo X, Liu L, Wang Y-C, Li J, Berbille A, Zhu L, et al. Tribovoltaic nanogenerators based on MXene-silicon heterojunctions for highly stable self-powered speed, displacement, tension, oscillation angle, and vibration sensors. Adv Funct Mater 2022;32:2113149.
- [18] Zhao C, Li Z, Fan T, Xiao C, Xie Y. Defects engineering with multiple dimensions in thermoelectric materials. Research 2020;2020:9652749.
- [19] Guo Q, Zhao Y, Tang Q, Duan J. Heat management strategy for all-inorganic, full-spectral concentrator CsPbBr₃/Bi₂Te₃-integrated solar cells. Sol RRL 2022;6:2200570.
- [20] Kumar S, Singh HH, Khare N. Flexible hybrid piezoelectric-thermoelectric generator for harnessing electrical energy from mechanical and thermal energy. Energy Convers Manag 2019;198:111783.
- [21] Gan YX. Recent development of thermoelectric nanofibers and their composites. J Materiomics 2023;9:99–130.
- [22] Zhang Z, Wang Z, Chen Y, Feng Y, Dong S, Zhou H, et al. Semiconductor contact-electrification-dominated tribovoltaic effect for ultrahigh power generation. Adv Mater 2022;34:2200146.
- [23] Ao D-W, Liu W-D, Chen Y-X, Wei M, Jabar B, Li F, et al. Novel thermal diffusion temperature engineering leading to high thermoelectric performance in Bi₂Te₃-based flexible thin-films. Adv Sci 2022;9:2103547.
- [24] Zheng Z-H, Shi X-L, Ao D-W, Liu W-D, Li M, Kou L-Z, et al. Harvesting waste heat with flexible Bi₂Te₃ thermoelectric thin film. Nat Sustain 2023;6:180–91.
- [25] Wei T-R, Wu C-F, Li F, Li J-F. Low-cost and environmentally benign selenides as promising thermoelectric materials. J Materiomics 2018;4:304–20.
- as promising thermoelectric materials. J Materiomics 2018;4:304–20. [26] Li D, Zhang BL, Ming HW, Wang L, Zu Y, Qin XY. Liquid-phase manipulation securing enhanced thermoelectric performance of Ag₂Se. ACS Appl Mater Interfaces 2021;13:34543–9.
- [27] Lin S, Guo L, Wang X, Liu Y, Wu Y, Li R, et al. Revealing the promising near-room-temperature thermoelectric performance in Ag₂Se single crystals. J Materiomics 2023;9:754–61.
- [28] Zhang Z, He T, Zhao J, Liu G, Wang ZL, Zhang C. Tribo-thermoelectric and tribovoltaic coupling effect at metal-semiconductor interface. Mater Today Phys 2021;16:100295.
- [29] Palaporn D, Mongkolthanaruk W, Tanusilp S, Kurosaki K, Pinitsoontorn S. A simple method for fabricating flexible thermoelectric nanocomposites based on bacterial cellulose nanofiber and Ag₂Se. Appl Phys Lett 2022;120: 073901.
- [30] Vlassenbroeck J, Masschaele B, Cnudde V, Dierick M, Pieters K, Van Hoorebeke L, et al. Octopus 8: a high performance tomographic reconstruction package for X-ray tube and synchrotron micro-ct. In: Desrues J, Viggiani G, Bésuelle P, editors. Advances in X-ray tomography for geomaterials. Wiley-ISTE; 2006. p. 167–73.
- [31] Limaye A. Drishti: a volume exploration and presentation tool. In: Stock SR, editor. Developments in X-ray tomography VIII, vol. 8506. San Diego, California, United States. SPIE: Proceedings of the SPIE Optical Engineering + Applications; 2012. 85060X. 2012 Aug 12-6.
- [32] Palaporn D, Kurosaki K, Pinitsoontorn S. Effect of sintering temperature on the thermoelectric properties of Ag₂Se fabricated by spark plasma sintering with high compression. Adv Energy Sustain Res 2023;4:2300082.
- [33] Ayele D. A facile one-pot synthesis and characterization of Ag₂Se nanoparticles at low temperature. Egypt J Basic. Appl Sci 2016;3:149–54.
- [34] Shahzad Shirazi M, Foroumadi A, Saberikia I, Moridi Farimani M. Very rapid synthesis of highly efficient and biocompatible Ag₂Se QD phytocatalysts using ultrasonic irradiation for aqueous/sustainable reduction of toxic nitroarenes to anilines with excellent yield/selectivity at room temperature. Ultrason Sonochem 2022;87:106037.
- [35] Mahato S, Kar AK. Structural, optical and electrical properties of electrodeposited cadmium selenide thin films for applications in photodetector and photoelectrochemical cell. J Electroanal Chem 2015;742:23–9.
- [36] Li L, Feng H, Wei X, Jiang K, Xue S, Chu PK. Ag as cocatalyst and electron-hole medium in CeO₂ QDs/Ag/Ag₂Se z-scheme heterojunction enhanced the photoelectrocatalytic properties of the photoelectrode. Nanomaterials 2020;10:253.
- [37] Dey N, Hsia KJ, Socie DF. The effects of grain size distribution on cavity nucleation and creep deformation in ceramics containing viscous grain boundary phase. Acta Mater 1997;45:4117–29.
- [38] Noisak J, Charoonsuk T, Pongampai S, Pinpru N, Pakawanit P, Vittayakorn W, et al. Towards the preparation of organic ferroelectric composites: fabrication of a gamma-glycine-bacterial cellulose composite *via* cold sintering process. J Mater Res Technol 2023;25:4749–60.
- [39] Ma J, Chen M, Qiao S, Chang J, Fu G, Wang S. Photovoltaic—pyroelectric coupled effect in Ag₂Se/Si heterojunction for broad-band, ultrafast, self-powered, position-sensitive detectors. ACS Photonics 2022;9:2160—9.
- [40] Indore NS, Karunakaran C, Jayas DS. Synchrotron tomography applications in agriculture and food sciences research: a review. Plant Methods 2022;18:101.
- [41] Xu X, Li J, Tao X, Yan Q, Wu H, Guan Z, et al. Study of interfacial design for direct-current tribovoltaic generators. Nano Energy 2022;94:106957.
- [42] Liu L, Li J, Ou-Yang W, Guan Z, Hu X, Xie M, et al. Ferromagnetic-assisted maxwell's displacement current based on iron/polymer composite for improving the triboelectric nanogenerator output. Nano Energy 2022;96: 107139.
- [43] Wortman JJ, Hauser JR, Burger RM. Effect of mechanical stress on p-n junction device characteristics. J Appl Phys 2004;35:2122–31.
- [44] Reddy PRS, Janardhanam V, Shim K-H, Reddy VR, Lee S-N, Park S-J, et al. Temperature-dependent Schottky barrier parameters of Ni/Au on n-type

- (001) β-Ga₂O₃ Schottky barrier diode. Vacuum 2020;171:109012.
- [45] Dogan H, Elagoz S. Temperature-dependent electrical transport properties of (Au/Ni)/n-GaN Schottky barrier diodes. Phys E Low-Dimens Syst Nanostructures 2014;63:186–92.
- [46] Whitten JE. Ultraviolet photoelectron spectroscopy: practical aspects and best practices. Appl Surf Sci Adv 2023;13:100384.
- [47] Tirado J, Vásquez-Montoya M, Roldán-Carmona C, Ralaiarisoa M, Koch N, Nazeeruddin MK, et al. Air-stable n—i—p planar perovskite solar cells using nickel oxide nanocrystals as sole hole-transporting material. ACS Appl Energy Mater 2019;2:4890—9.
- [48] Chuang C-HM, Brown PR, Bulović V, Bawendi MG. Improved performance and stability in quantum dot solar cells through band alignment engineering. Nat Mater 2014;13:796–801.
- [49] Bui D-P, Pham M-T, Tran H-H, Nguyen T-D, Cao TM, Pham VV. Revisiting the key optical and electrical characteristics in reporting the photocatalysis of semiconductors. ACS Omega 2021:6:27379—86.
- [50] Eastment RM, Mee CHB. Work function measurements on (100), (110) and (111) surfaces of aluminium. J Phys F Met Phys 1973;3:1738.
- [51] Li X, Lu Y, Cai K, Gao M, Li Y, Wang Z, et al. Exceptional power factor of flexible Ag/Ag₂Se thermoelectric composite films. Chem Eng J 2022;434:134739.
- [52] Wu H, Shi X-I, Duan J, Liu Q, Chen Z-G. Advances in Ag₂Se-based thermoelectrics from materials to applications. Energy Environ Sci 2023;16: 1870–906.
- [53] Ikegami T, Maezono T, Nakanishi F, Yamagata Y, Ebihara K. Estimation of equivalent circuit parameters of PV module and its application to optimal operation of PV system. Sol Energy Mater Sol Cells 2001;67:389—95.
- [54] Boyd MT, Klein SA, Reindl DT, Dougherty BP. Evaluation and validation of equivalent circuit photovoltaic solar cell performance models. J Sol Energy Eng 2011;133.
- [55] Jaziri N, Boughamoura A, Müller J, Mezghani B, Tounsi F, Ismail M. A comprehensive review of thermoelectric generators: technologies and common applications. Energy Rep 2020;6:264–87.
- [56] Xia J, Luo X, Li J, Zhu L, Wang ZL. Wear-resisting and stable 4H-SiC/Cu-based tribovoltaic nanogenerators for self-powered sensing in a harsh environment. ACS Appl Mater Interfaces 2022;14:55192–200.
- [57] Nagarajan PK, Subramani J, Suyambazhahan S, Sathyamurthy R. Nanofluids for solar collector applications: a review. Energy Proc 2014;61:2416–34.
- [58] Wen J, Khonsari MM. On the temperature rise of bodies subjected to unidirectional or oscillating frictional heating and surface convective cooling. Tribol Trans 2009;52:310–22.
- [59] Chen X, Jiang T, Sun Z, Ou-Yang W. Field emission device driven by self-powered contact-electrification: simulation and experimental analysis. Appl Phys Lett 2015:107:114103.
- [60] Yang R, Benner M, Guo Z, Zhou C, Liu J. High-performance flexible Schottky dc generator via metal/conducting polymer sliding contacts. Adv Funct Mater 2021;31:2103132.
- [61] Meng J, Guo ZH, Pan C, Wang L, Chang C, Li L, et al. Flexible textile directcurrent generator based on the tribovoltaic effect at dynamic metalsemiconducting polymer interfaces. ACS Energy Lett 2021;6:2442–50.
- [62] Wilken S, Scheunemann D, Dahlström S, Nyman M, Parisi J, Österbacka R. How to reduce charge recombination in organic solar cells: there are still lessons to learn from P3HT:PCBM. Adv Electron Mater 2021;7:2001056.
- [63] Blendell JE, Handwerker CA. Ceramics: grain growth. In: Buschow KHJ, Cahn RW, Flemings MC, Ilschner B, Kramer EJ, Mahajan S, et al., editors. Encyclopedia of materials: science and technology. Oxford: Elsevier; 2001. p. 1105–8.
- [64] Šutka A, Malnieks K, Zubkins Mr, Pludons Ar, Šarakovskis A, Verners O, et al. Tribovoltaic performance of TiO₂ thin films: crystallinity, contact metal, and thermoelectric effects. ACS Appl Mater Interfaces 2023;15:33140–7.
- [65] Yang D, Zhang L, Luo N, Liu Y, Sun W, Peng J, et al. Tribological-behaviour-controlled direct-current triboelectric nanogenerator based on the tribovoltaic effect under high contact pressure. Nano Energy 2022;99:107370.
- [66] Huang X, Xiang X, Nie J, Peng D, Yang F, Wu Z, et al. Microscale Schottky

- superlubric generator with high direct-current density and ultralong life. Nat Commun 2021;12:2268.
- [67] You Z, Wang S, Li Z, Zou Y, Lu T, Wang F, et al. High current output directcurrent triboelectric nanogenerator based on organic semiconductor heterojunction. Nano Energy 2022;91:106667.
- [68] Yuan H, Xiao Z, Wan J, Xiang Y, Dai G, Li H, et al. A rolling-mode Al/CsPbBr₃ Schottky junction direct-current triboelectric nanogenerator for harvesting mechanical and solar energy. Adv Energy Mater 2022;12:2200550.
- [69] Ouslimane T, Et-taya L, Elmaimouni L, Benami A. Impact of absorber layer thickness, defect density, and operating temperature on the performance of MAPbl₃ solar cells based on ZnO electron transporting material. Heliyon 2021;7:e06379.
- [70] Ahmed MAM, Meyer WE, Nel JM. Investigation of the structural and temperature-dependent electrical properties of MZnO (M = Ce and Sm) Schottky diode devices fabricated using the sol—gel spin-coating technique. I Mater Sci Mater Electron 2023;34:1312.



Miss Supakarn Worathat is a Master candidate in Applied Chemistry at KMITL in Thailand. She completed her Bachelor's degree in Industrial Chemistry from the same institution in 2022. Her research interests are focused on Tribovoltaic Nanogenerator and the Tribovoltaic effect.



Dr. Saichon Sriphan is currently an Associate Professor in Materials Science with Faculty of Science, Energy and Environment, King Mongkut's University of Technology North Bangkok, Thailand. He received the Ph.D. degree in Electrical Engineering from Naresuan University Thailand in 2017. He held a post-doctoral researcher at the Advanced Materials Research (AMR) Unit, School of Science, King Mongkut's Institute of Technology Ladkrabang, Thailand. His research interests mainly focus on developing novel harvesting/sensing devices, coupling mechanism in hybrid energy harvesters, and energy material characterizations.



Dr. Naratip Vittayakorn is a Professor of Materials Science and a director of Advanced Materials Research (AMR) at King Mongkut's Institute of Technology Ladkrabang (KMITL), Thailand. He obtained his Ph.D. degree from Chiang Mai University, Thailand, and was a visiting scientist at lowa State University from 2003 through 2005. With over 300 scientific papers and 5 patents, his research mainly focuses on electroceramics, piezoelectric, triboelectric nanogenerators, and energy harvesting materials.